Progress in Organic Coatings 128 (2019) 1–10

Contents lists available at ScienceDirect

Progress in Organic Coatings

journal homepage: www.elsevier.com/locate/porgcoat

Functionalized zirconia compounds as antifungal additives for hygienic waterborne coatings

Romina A. Arreche[a,*], Katerine Igal[a], Natalia Bellotti[b], Cecilia Deyá[b], Patricia G. Vázquez[a]

[a] CINDECA - Centro de Investigación y Desarrollo en Ciencias Aplicadas, Dr. Jorge J. Ronco, CCT La Plata, CONICET - Departamento de Química, Facultad de Ciencias Exactas, UNLP, 47 No 257 Buenos Aires, 1900, La Plata, Argentina

[b] CIDEPINT - Centro de Investigación y Desarrollo en Tecnología de Pinturas (CIC – CONICET-UNLP), Calle 52 e/121 y 122, Buenos Aires, 1900, La Plata, Argentina

ARTICLE INFO

Keywords:
Silica
Zirconia
Silver
Antimicrobial additives
Hygienic coatings
Bio-resistance

ABSTRACT

The addition of silver (Ag) into the chemical synthesis of materials, transform them into materials technologically relevant to be used as antimicrobial additives. In this work, the sol-gel method was used to obtain materials based on silica and zirconia, with the inclusion of Ag. The solids were characterized by potentiometric titration, specific surface area (S_{BET}), X-Ray diffraction (XRD), Fourier transform infrared spectroscopy (FTIR), scanning electron microscopy (SEM) and transmission electron microscopy (TEM) and, the antifungal activity of the additives was assessed by agar plate inhibition against *Chaetomium globosum* and *Alternaria alternata*. In addition, the resistance to fungal growth on waterborne coatings was evaluated after the incorporation of the solids into paint formulation.

Amorphous materials with different acidic and textural properties were obtained. Most of the tested solids showed antifungal activity at the highest concentration used, and the presence of Ag increased the percentage of inhibition. The mixed oxides Ag-additives improved the antifungal activity compare with the pure Ag-oxides (silica or zirconia). In this sense, a synergic effect between zirconia/silica and silver would be a promising result that would reduce the amount of silver in these bioactive materials. This work was performed as a preliminary study, in order to guide the selection of a suitable additive from a list of possible antifungal agents.

1. Introduction

Controlled microbial growth on indoor surfaces constitutes an important issue for a healthy human development. In recent years, more evidence has associated biofilms with persistent infections and it is believed that ~80% of the cases reported in the United States are related with this [1]. Many pathogens are persistent in the environment from hours to months and frequently contaminate the surface environment [2]. Among the microorganisms that manage to form biofilms on indoor paint films, fungi are the most deteriorating and resistant. They can grow in a wide pH range and are extremely resistant to drying, remaining active at moisture levels too low for bacteria [3,4]. Antimicrobial coatings represent an alternative to deal with this problem. In the past, organomercury compounds, chlorinated phenols, and organotin compounds were often used, but these environmentally harmful products are now being replaced [5]. In this sense, new eco-friendly materials need to be developed to control and prevent the microbial contamination [6]. The synthesis of silica is an alternative, according with the trend of new antimicrobial formulation to replace traditional additives. On the other hand, zirconia compounds have attractive properties and found applications in dental implants, knee and hip replacements, deodorant and antiperspirant preparations. Besides, experimental and clinical studies support that Zr compounds are biocompatible and exhibit low toxicity [7,8]. A possible approach to design antimicrobial surfaces is to incorporate bioactive additives based on functionalized silica matrix [9,10]. These frameworks associated with metallic particles like silver or copper have been studied previously and used as antimicrobial fillers with acceptable results against fungal and bacterial strains [11–13].

Silver nanoparticles (NPs) have showed a broad spectrum of antimicrobial activity although the mechanism of action is not entirely known [14,15]. There are different cellular target to Ag ions and NPs, such as: cell membrane, DNA, proteins, electron transport, nutrient uptake, protein oxidation, or membrane potential [16–18]. Several of the cited effects are based on the interaction of silver with sulfur-containing proteins and the phosphorus-containing molecules [19]. These kind of chemical interactions are expected to be found in both bacteria and fungi. Although there are less published data about fungi, some

* Corresponding author.
E-mail address: arrecheromina@quimica.unlp.edu.ar (R.A. Arreche).

https://doi.org/10.1016/j.porgcoat.2018.12.004
Received 11 January 2018; Received in revised form 30 November 2018; Accepted 1 December 2018

studies found that specifically silver nanoparticles inhibit spores germination of *Fusarium* species [20]. Kim et al. showed that AgNPs affected *Candida albicans* cells by attacking their membranes, thus disrupting membrane potential [21] and, recent studies documented AgNPs mediated inhibition of carcinogenic mycotoxin and secondary metabolite from *Aspergillus parasiticus* [22].

The advantage using an oxide matrix associated with an antimicrobial agent resides in its protective function that lead to a longer useful life of the material obtained maintaining its bioactivity over time. Besides, the sol-gel method is an appropriated way to obtain this immobilization [10,23].

Related to the exposed above, the aim of the present work was to obtain bioactive additives with zirconia using the sol-gel method, and incorporate them in waterborne paints, in order to obtain antimicrobial coatings. The materials synthesized were characterized by potentiometric titration, specific surface area (S_{BET}), X-Ray diffraction (XRD), Fourier transform infrared spectroscopy (FTIR), scanning electron microscopy (SEM) and transmission electron microscopy (TEM). Then, the antifungal activity of the solids was assessed against *Chaetomium globosum* (KU936228) and *Alternaria alternata* (KU 936,229), obtained previously from biodeteriorated coatings [24]. These fungi were selected for their ability to grow on indoor surfaces and to be negative to human health due to produce a variety of different compounds including mycotoxins [25–27]. Finally, seven paints were formulated with the addition of the synthesized solids as additives and the bioresistance assay was carried out by a procedure similar to the standard method ASTM D5590 [28]. Taking into account that silver may be oxidized by light, paint color parameters were evaluated against time.

This work is focused on the preparation of new materials that can provide solutions to the technological and environmental challenges in different areas.

2. Materials and methods

2.1. Synthesis of the additives

The sol-gel method under N_2 atmosphere was carried out to synthesize the additives. Different silicas, zirconias and mixed oxides were prepared with a silver salt as antimicrobial active agent. Tetraethoxysilane (TEOS) (98%, Aldrich) and zirconium *n*-propoxide ($Zr(OPr)_4$) (70%, Aldrich) were used as precursor of the siliceous and zirconium oxides, respectively, and both, in equal molar amounts, were used to obtain mixed oxides; acetic acid (AcH) (CH_3CO_2H - 99.7%, Anedra) and phosphomolybdic acid (PMA) ($H_3[P(Mo_3O_{10})_4]xH_2O$, Fluka) were used as catalysts, in order to assess their influence on the final structure of the solids, and absolute ethanol (C_2H_5OH - 99.99%, Carlo Erba) and distilled water were used as solvents in all the synthesis. Silver acetate (AgAc) (CH_3CO_2Ag - 99.99%, Aldrich) was added in selected solids in order to reach a concentration of 1%wt. in the dry solid. For the synthesis, half of solvent was put into a beaker with the catalyst (acetic acid or PMA), then the precursor was incorporated (TEOS, $Zr(OPr)_4$ or both) and the remaining amount of ethanol was added. Silver acetate was incorporated in selected samples and, afterwards, the slow addition of water was carried out. Only in silica samples the addition of water was possible, in zirconia samples this addition resulted in an instant hydrolysis of the precursor in the reaction mixture, yielding an opaque solid. The mixture was stirred for 2 h and, finally, the wet gel particles were dried at room temperature and atmospheric pressure up to the complete solidification. To obtain dry samples, a thermal treatment at low temperature 150 °C for 2 h was used. In the samples synthesized with acetic acid, the molar ratio of the reagents was 1:1.16:5:3.7 for precursor:catalyst:solvent:water respectively, whereas in those prepared with PMA, the addition of the catalyst was done in order to reach a final concentration into the silica of 11 wt. % of PMA [29,30], and the molar ratio of the reagents was 1:0.005:5:3.7. The composition and nomenclature of the synthesized solids are given in Table 1 and, in accordance with the compositions the following meanings were adopted: S = silica, Z = zirconia, SZ = silica-zirconia, A = acetic acid, H = heteropolyacid and, Ag = silver.

Table 1
Compositions of starting solutions (molar ratio) and nomenclature of the solids.

Sample	TEOS	$Zr(OPr)_4$	AcH	PMA	C_2H_5OH	H_2O	AgAc
SA	1	–	1.16	–	5	3.7	–
SH	1	–	–	0.005	5	3.7	–
SA-Ag	1	–	1.16	–	5	3.7	0.008
SH-Ag	1	–	–	0.005	5	3.7	0.008
ZA	–	1	1.16	–	5	–	–
ZH	–	1	–	0.005	5	–	–
ZA-Ag	–	1	1.16	–	5	–	0.008
ZH-Ag	–	1	–	0.005	5	–	0.008
SZA	0.5	0.5	1.16	–	5	–	–
SZH	0.5	0.5	–	0.005	5	–	–
SZA-Ag	0.5	0.5	1.16	–	5	–	0.008
SZH-Ag	0.5	0.5	–	0.005	5	–	0.008

2.2. Characterization of the additives

2.2.1. Potentiometric titration with n-butylamine

The acidic properties of the solids were evaluated by potentiometric titration with *n*-butylamine, in a Metrohm 794 Basic Titrino titrator (Switzerland) with a double-junction electrode. First, 0.025 g of sample was suspended in 45 mL of acetonitrile and stirred for 540 s and second, 0.025 mL/min of an *n*-butylamine solution in acetonitrile (0.025 N) was added, while stirring constantly.

2.2.2. Textural properties

The textural properties of the additives, such as the specific surface area (S_{BET}), the pore volume and pore size, were determined by adsoption/desorption in Micromeritics Accusorb 2100 equipment (USA), using N_2 as absorbable gas at 77 K. Before the measurement, each sample was degassed at 100 °C for 12 h and under 30 mmHg.

2.2.3. X-ray diffraction

The X-Ray diffraction (XRD) diagrams were obtained in Philips (Holland) PW-1390 (channel control) and PW-1394 (motor control) equipment coupled to a scanning graphical recorder, using Cu Kα (α = 1.5417 Å) radiation, Ni filter, 20 mA and 40 kV in the voltage source, a 5–60 2θ scanning angle range, a scanning rate of 2°/min and 2000 counts/s for the amplitude of the vertical scale.

2.2.4. Fourier transform infrared spectroscopy

FT-IR spectra were obtained using Bruker Vertex 70 equipment (Germany) and pellets of the sample in KBr (Aldrich, 99 wt% FT-IR purity), measured in a range between 400 and 4000 cm^{-1} at room temperature. Two hundred scans were collected at a resolution of 4 cm^{-1} and averaged.

2.2.5. Scanning electron microscopy

Scanning electron microscopy (SEM) was used to obtain different micrographs of the additives, in Philips 505 equipment (Holland), using a voltage of 15 kV. Samples were supported on graphite and metallized with a sputtered gold film. The micrographs were obtained with an ADDAII acquisition device (Soft Imaging System).

2.2.6. Transmission electron microscopy

Transmission electron microscopy (TEM) was performed with a JEOL microscope (100 CX) (Japan), with an accelerating voltage of 100 kV. Samples were prepared by their suspension in ethanol and placing an aliquot over carbon-coated copper grids, allowing the samples to dry in a desiccator for 30 min at room temperature.

X-ray mapping was acquired by using a Talos F200X HR-TEM

microscope operating at 200 kV equipped with a SuperX EDS spectrometer (composed by 4 EDS SDD detectors).

2.2.7. Antifungal activity

Fungal strains, *Alternaria alternata* (KU 936229) and *Chaetomium globosum* (KU936228), previously isolated from bio-deteriorated surfaces [31] were used to evaluate the antifungal activity. These strains were selected for their ability to grow on indoor surfaces and to be negative to human health due to produce a variety of different compounds including mycotoxins [25–27]. *A. alternata* spores are one of the most frequently characterized fungal spore types in the atmosphere [32] and their ability to produce an important variety of allergenic compounds is related to severe exacerbations of asthma in children and young adults [33]. On the other hand, *C. globosum* fungi are known to produce cellulolytic compounds that degrade and decompose the cellulose thickeners present in waterborne paints [34] as well as to produce secondary metabolites with intravenous toxicity demonstrated in animal test [35].

The antifungal activity of the additives was evaluated in vitro by assessing the fungal growth inhibition on agar plates [36] and employing different concentrations of the solids. Fungal spores were removed from Petri dishes cultures and then suspended in physiological solution containing 0.85% w/v NaCl and 0.005% w/v Tween 20. The concentration of the suspension was adjusted to 0.3-0.5 $\times 10^5$ spores/mL employing a Neubauer chamber. Plates with 15 mL of solid culture medium (CM-agar: 1.5 g agar; 1 g dextrose; 0.5 g peptone; 0.1 g KH_2PO_4; 0.05 g $MgSO_4$ $7H_2O$; and 100 mL of distilled water) were prepared containing the selected additive and were inoculated with 20 µL of the spores´ suspension. Three different concentrations of Ag, included in the additives, were evaluated, 0.001% Ag (w/v), 0.01% Ag (w/v) and 0.05% Ag (w/v), as well as the control (without Ag) and the other without the addition of any antimicrobial agent (only CM-agar). Duplicates were set up for each concentration, including the controls. After the inoculation of each fungal suspension in a single point located at the center, the plates were incubated at 26 °C and the fungal growth was evaluated after 10 days. The average diameter of fungal colony was recorded and the inhibition effect was calculated according to the equation (1) [37,38]:

$$\text{Inhibition (\%)} = [1 - (\text{radial growth with solid/radial growth of control})] \times 100 \quad (1)$$

Three measurements of the fungal growth diameter were made in each plate and standard deviation was determined [36].

2.3. Coatings bio-resistance assay

Three of the solids synthesized with silver were selected due to be those with highest antifungal activity, taking into account bioassays realized previously. In addition, paints with solids without silver were made too. Therefore, seven waterborne acrylic-styrene paints were prepared in order to evaluate and compare their antifungal properties; one of the paints was prepared as control, without any antimicrobial additive, and six paints were prepared with similar formulation, but adding the experimental antifungal additives at a concentration of 5 g for 100 g of paint. The resin used was an acrylic-styrene one (Thyosil E190, Diransa). Table 2 shows the composition of the paints used in this study (in wt. %). The preparation was done with a high speed disperser and then two layers of paint were spread into glass slides and dried for 15 days under dark condition before testing. The glasses were cut in squares of 2.5 cm × 2.5 cm and irradiated with germicide UV Philips light (20 W), for 40 min each side to decontaminate the surface before test and to avoid the growth of other microorganisms. The painted glasses were placed in mineral media (5 g NaCl, 1 g HK_2PO_4, 1 g $(NH_4)H_2PO_4$, 1 g $(NH_4)_2SO_4$, 0.2 g $MgSO_4$, 3 g KNO_3, 15 g of agar and up to 1000 mL of distilled water) and inoculated homogeneously and all over the painted surface with 50 µL of a spore suspension (10^5 spores/mL) of each fungal species. The glasses were incubated at 28 °C and, after 4 weeks, were evaluated according to ASTM D5590 standard specification [28], that states a degree of fungal growth according to: none, trace of growth (< 10%), light growth (10–30%), moderate growth (30–60%), heavy growth (60–100%) rating as 0, 1, 2, 3 and 4, respectively.

Table 2
Composition of the formulated paints (in wt. %).

Function	P Control	P Additive
Solvent (Water)	26.80	26.80
Defoamer	0.27	0.27
Thickener	0.55	0.55
Dispersant	0.47	0.47
Humectant	0.05	0.05
Resin	7.20	7.20
Pigment	19.80	19.80
Filler	42.10	37.10
Preservative	0.25	0.25
Coalescent	1.88	1.88
Deodorant	0.63	0.63
Additive x*	–	5.00

*x = SA, SH-Ag (1%wt. Ag), ZA, ZH-Ag (1%wt. Ag), SZA and SZH-Ag (1%wt. Ag).

2.3.1. Observation of the paints by scanning electron microscopy (SEM)

Surface observation of the paint films was carried out by SEM before and after the bio-resistance assay, by Philips 505 equipment, using a voltage of 15 kV, supporting the samples on graphite and covering with gold. The images were obtained with an ADDAII acquisition device (Soft Imaging System).

2.4. Color and gloss measurements of the coatings

CIElab color parameters were evaluated on cured paints during their sunlight exposure through a window and in the darkness. The CIElab parameter L* represent the luminosity of the color which varies from 0 to 100 (white) while a* and b*, the variation magenta–blue green (a*) and yellow–blue (b*). The change of color (ΔE) is calculated as [39].

$$\Delta E = [(a - a_0)^2 + (b - b_0)^2 + (L - L_0)^2]^{1/2}$$

being a_0, b_0 and L_0, the CIElab parameters of the painted panels at t = 0 and a, b and L, the values corresponding as time elapsed. Visual appearance and ΔE can be related with the rating in Table 3 [39]. Gloss parameters were also evaluated. Measurements were done employing a By K Gardner gloss-meter.

3. Results and discussion

3.1. Characterization of the additives

A color change of the solids was observed according to the composition of the synthesis (Table 1). When acetic acid was used, the silica

Table 3
Relationship between visual assessment and ΔE differences.

ΔE	Assessment of color differences
< 0. 2	No visible
0.2–0.5	Very slightly
0.5–1.5	Slightly
1.5–3.0	Evident
3.0–6.0	Very evident
6.0–12.0	Big
> 12.0	Very big

Table 4
Acidity and textural properties of the solids synthesized.

Sample	E_i (mV)	S_{BET} (m^2/g)[a]	Pore volume (cm^3/g)[b]	Pore size (Å)[c]
SA	135.5	464.0	0.2	18.7
SH	463.6	220.5	0.1	22.7
SA-Ag	59.5	451.8	0.2	19.6
SH-Ag	98.6	316.3	0.2	18.5
ZA	−58.2	11.2	–	34.8
ZH	19.2	50.3	–	25.6
ZA-Ag	−179.2	201.0	0.1	19.6
ZH-Ag	−126.4	203.6	0.1	19.9
SZA	101.1	2.2	–	–
SZH	177.2	188.6	–	19.8
SZA-Ag	97.0	260.8	0.1	20.0
SZH-Ag	185.8	250.2	0.1	18.9

[a] Surface area calculated by the BET method (pressure range 0–1 p/p°).
[b] Pore volume (calculated at p/p° = 0.99).
[c] Pore diameter calculated by using the adsorption average pore width (4 V/A by BET).

obtained was translucent; whereas the zirconia was yellowish due to the precursor color. In the case that PMA was used as catalyst, greenish crystals of silica were obtained, whereas whitish solids were visualized for zirconia and mixed oxides and different solid phases was observed. This distinctive morphology and color suggest that the primary structure (Keggin) of the phosphomolybdic acid was mainly destabilized. When silver acetate was added in the synthesis using acetic acid as catalyst, a brown coloring was observed. Ritzer et al. [40] studied the darkening of silica glasses doped with silver by the sol-gel method and they observed that along with the preparation and solidification of the gels, the silver added is reduced to Ag° and form aggregates, which give a yellowish-brown coloring.

Table 4 shows the initial electrode potential (E_i), the specific surface area (S_{BET}), the pore volume and the mean pore size measured of the additives synthesized. The potentiometric titration allows the determination of the acidic properties of a dispersion of solid particles by measuring the electrode potential through the membrane. The initial electrode potential (E_i) indicates the maximum acid strength of the sites, and it may be classified according to the following scale: very strong sites, $E_i > 100$ mV; strong sites, $0 < E_i < 100$ mV; weak sites, $-100 < E_i < 0$ mV; and very weak sites, $E_i < -100$ mV [30,41]. When PMA were used as catalyst in the synthesis compare with acetic acid, an increase of the acidity was observed, and this difference could be attributed to the initial acidic strength extremely high (800 mV) of PMA [30].

In general, when silver was incorporated into the synthesis, a decrease of the E_i values was observed. In samples synthesized with AcH as catalyst, this decrease could be due to the common ion effect, and the addition of acetate ions from the silver acetate salt would produce the suppression of the degree of dissociation of the weak electrolyte from the acetic acid. On the other hand, in samples synthesized with PMA as catalysts, with the addition of Ag to the synthesis, monoprotic acidic sites were maintained, but the initial acidity decreased by the substitution of PMA protons by silver.

As is shown in Table 4, the specific surface area (S_{BET}) of silica samples decreased when PMA was included into the oxide, due to S_{BET} values of PMA are low, between 3 and 10 m^2/g [29]. Popa et al. [42] reported equivalent results when PMA is supported in mesoporous silica. The zirconium oxides did not present significant specific surface areas, and showed S_{BET} values very low, almost coincident with the error of the technique (error range of about ± 10 m^2/g nitrogen adsorbed). But, in zirconia and mixed oxide samples, when PMA was included as catalyst in the synthesis, the S_{BET} values increased notably, by steric effects. In the same way, in Ag-samples, when it was involved the formation of a silver salt of acid, the surface area increased by steric effects, as the radius of the compound included increased, i.e. acid

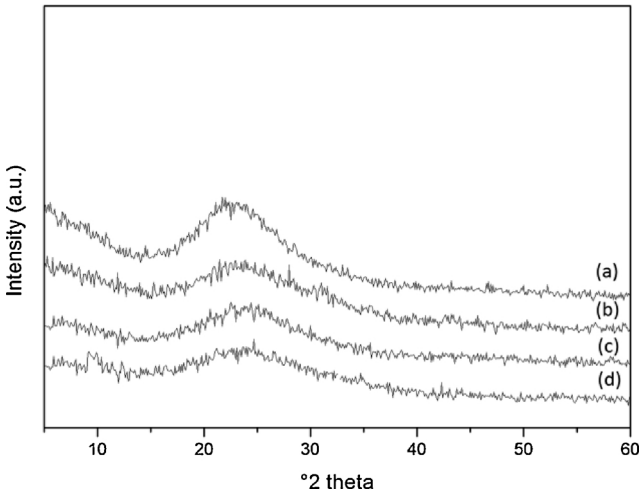

Fig. 1. XRD diagrams of the samples, (a) SA-Ag, (b) SA, (c) SH-Ag and (d) SH.

compared to the salt, and intra-molecular spaces are greater. Both silica samples, those synthesized with acetic acid as with PMA, showed type I isotherms, characteristic of microporous solids, with a large isotherm plateau, and the zirconia and mixed oxides showed type II isotherms, indicating solids with pore diameters larger than micropores [43].

The XRD diagrams of the samples indicated their amorphous nature. Fig. 1 shows the XRD patterns for the silica-additives, SA, SA-Ag, SH and SH-Ag, with a broad hump around 2Θ ~23, typical of this materials [44]. The absence of Ag peaks in the samples SA-Ag and SH-Ag can be attributed to highly disperse silver species.

The functional groups present in the additives synthesized were identified by FT-IR. Fig. 2a and b shows the FT-IR spectra of the oxides using acetic acid as catalyst and PMA, respectively. The IR spectra of silica showed four absorption bands around 1200, 1080, 800 and 460 cm^{-1}, which are characteristic of this oxide [45]. Bands at 1200 and 1080 cm^{-1} are assigned to asymmetric stretching modes of the Si—O—Si bond and, the vibration at 800 cm^{-1} is associated with the symmetric stretching of the Si—O—Si bond or vibrational modes of ring structures. At lower wavenumber values, the 460 cm^{-1} band is assigned to the Si-O-Si bending mode, although it may be associated with defects caused by non-symmetric links [46].

Three additional bands characteristic of silica obtained by sol-gel method were observed, in the range 3600-3000 cm^{-1}, 1640 cm^{-1} and 950 cm^{-1}. The characteristic broadband, in the range of 3600-3000 cm^{-1}, is assigned to the stretching vibrations of water molecules with bridged-hydrogen bonds and silanol groups (OH and SiO—H) on the surface of the silica [47]. The second band (1640 cm^{-1}) is assigned to the molecular water deformation and this result from the angular deformations of O—H in H_2O (H—O—H). This band is associated with the water adsorption on the surface of synthesized sample. The presence of these two bands indicates that xerogel silica contains a high amount of molecular water and hydroxyls. There is a small band near 1650 cm^{-1}, which may be due to residual ethanol and finally, the band centered around 950 cm^{-1} is assigned to the vibration of Si—OH (silanols) bonds [47].

FT-IR spectra of ZrO_2 showed an absorption bandwidth between 3700-3000 cm^{-1} corresponding to the stretching vibration of OH (ν(OH)), related to free water (absorbed surface and capillary water) [48] and a band at 1560 cm^{-1} corresponding to the vibration of scissor of OH, in the plane (δs(OH)). The signal belonging to C—H bonds, around 1340 cm^{-1}, identifies organic matter retained in the solid after calcination and the band at 1027 cm^{-1} is attributed to the presence of propoxide groups of the precursor used. The characteristic bands of the symmetrical stretching vibrations νs (O—Zr—O) and asymmetric νas (O—Zr—O) of the ZrO_2 occur in the 800-850 cm^{-1} region. On the other

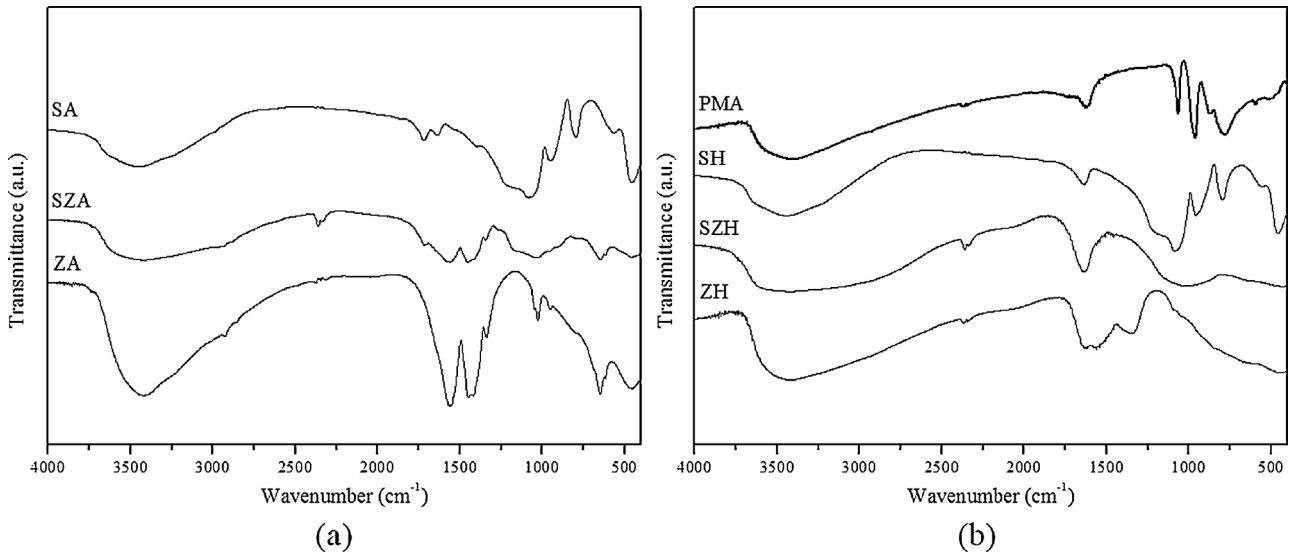

Fig. 2. FTIR spectra of the additives synthesized with (a) acetic acid and (b) PMA as catalyst.

hand, the signals located between 800 and 500 cm^{-1} correspond to Zr—O stretches indicating the formation of zirconium oxide [49,50].

Fig. 2b shows the FT-IR spectra of the oxides using PMA as catalyst and, an analysis of the conservation of the structure within the obtained matrices was carried out. The FT-IR spectra of phosphomolybdic acid has been previously studied and the main characteristic bands are observed at 1064 cm^{-1} for (P—O_a), 964 cm^{-1} for (Mo = O_d), 871 cm^{-1} for (Mo-O_b-Mo) and 784 cm^{-1} for (Mo—O_c—Mo) [51]. The vibrational spectrum of PMA bulk, with Keggin primary structure, is modified according to the nature of the elements that surround it. In Fig. 3 is observed that the PMA bands are preserved in the siliceous sample (SH), although they are wider and are partially overlapping with the intense absorption bands that the silicon oxides present. In ZH and SZH samples, the characteristic bands of bulk PMA are not observed, suggesting that a structural destabilization was produced on the heteropolyacid present in the samples.

The materials were examined by SEM to evaluate morphological changes with the use of different catalysts and, the structure of silica, zirconia and mixed oxides. A broad size distribution of particles in all the samples, mainly with diameters in the range of less than 10 μm, and some bigger particles were observed. The morphology of the samples synthesized with acetic acid was different compared with those obtained with phosphomolibdic acid. Samples synthesized with AcH (SA, SA-Ag, ZA, ZA-Ag, SZA and SZA-Ag) presented a laminar morphology typical of pure silica, whereas those synthesized with PMA (SH, SH-Ag, ZH, ZH-Ag, SZH, SZH-Ag) showed agglomerate particles. Smaller sizes

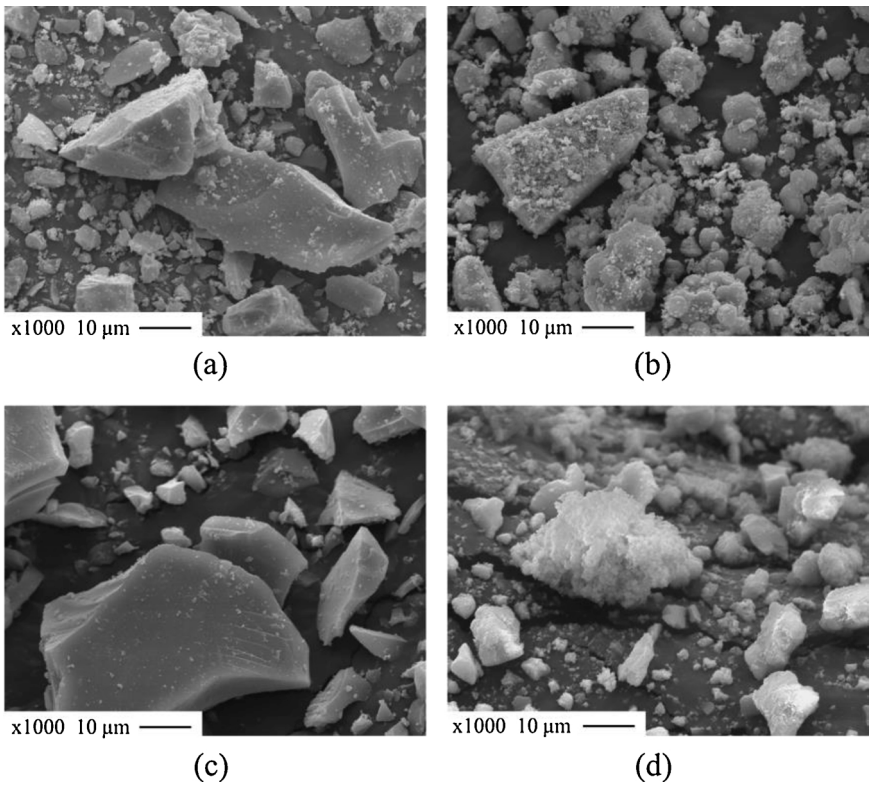

Fig. 3. SEM micrographs of zirconia and mixed oxides synthesized with acetic acid: (a) ZA and (c) SZA; and phosphomolybdic acid: (b) ZH and (d) SZH (Bar: 10 μm).

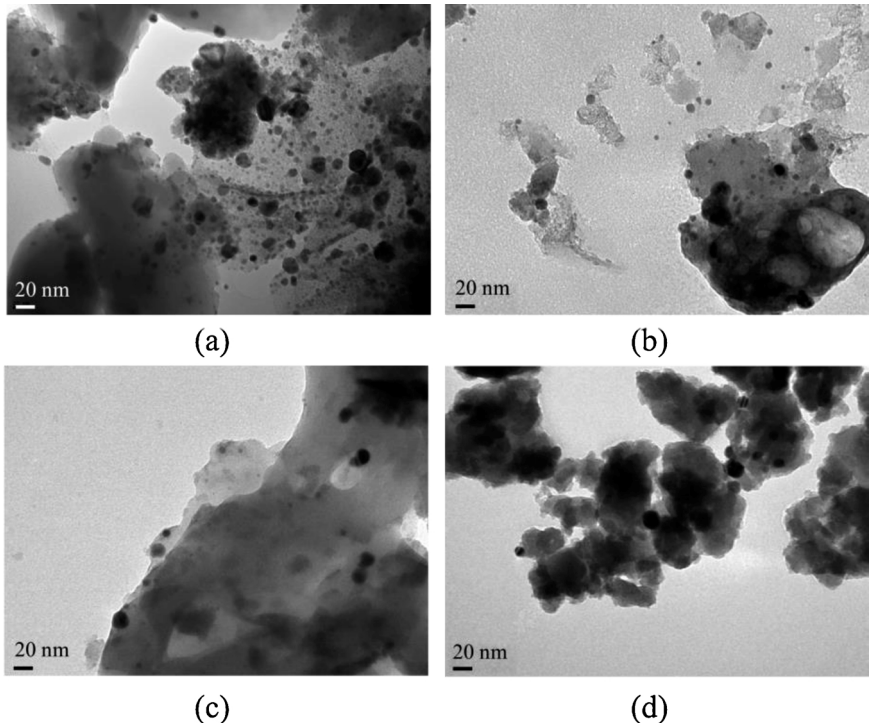

Fig. 4. TEM micrographs of Ag-silica additives, (a) SA-Ag, (b) SH-Ag, and Ag-mixed oxides additives (c) SZA-Ag, (d) SZH-Ag (Bar: 20 nm).

of particles were observed in zirconia samples compare with silica samples, no matter which of the catalyst was used. As example, Fig. 3 shows SEM micrographs of ZA, SZA, ZH and SZH oxides.

By TEM, silver nanoparticles can be clearly seen embedded in the oxide matrix being essentially spherical in shape and well distributed in the amorphous oxide matrix, with sizes between 5 and 30 nm (Fig. 4). According to the TEM micrographs, the materials without Ag in its matrix, showed the same oxide particles morphology to those with this element. In relation to the results obtained by TEM, can be concluded in agreement with Adegboyega et al. [52] that silver salts in the presence of organic acids (fulvic or humic acid) help the formation of silver nanoparticles due to the reduction of silver ions (Ag^+) by the functional groups found in the organic matter. Specifically, the presence of free radicals and carboxylic or phenolic groups would be responsible for the formation of Ag_2O from Ag^+. In addition, exposure to UV light results in the formation of Ag nanoparticles with the characteristic yellow color in presence of organic acids acting as photosensitizers in the formation of nanoparticles. Babapour et al. [53] studied the inclusion of silver in a silica matrix through the sol-gel technique and analyzed the materials by X-ray photoelectron spectroscopy (XPS) to elucidate the chemical state of silver nanoparticles on the surface. They observed that at 100 °C the silver particles have a high tendency to accumulate in the surface but, at higher temperatures, the diffusion of the particles from the surface to the matrix takes place. In addition, they found that in the dry samples (in air at 100 °C) more than 90% of the concentration of Ag on the surface is in the Ag° (metallic) state. However, after treating the materials thermally at 200 °C, the silver particles are oxidized and an increase in the surface concentration of Ag^+ and $Ag_2{}^+$ is observed. This continues to grow up to 400 °C and the results are independent of the silver concentration in the siliceous matrix.

X-ray mapping and high-resolution TEM (HRTEM) images of samples SH-Ag, SZA-Ag and SZH-Ag confirm the formation of silver nanoparticles. A homogeneous distribution of the components in the oxides matrix was observed and the figures nicely illustrates that most of the particles were spherical. As example, Fig. 5 shows the elemental mapping of SZH-Ag sample, showing: silver, silicon, oxygen, molybdenum and zirconium. Elemental mapping of SH-Ag, SZA-Ag samples are showed as Supplementary Information (Figs. S1 and S2, respectively).

3.2. Antifungal activity

The influence of the synthesized additives on the growth of *A. alternata* and *C. globosum* strains was assessed by measuring the diameters of the fungal growth on CM-agar, after 10 days of incubation at 26 ± 2 °C. Table 3 shows the average growth diameter with the different concentrations of the additives against both fungi, and as example, Fig. 6 shows the fungal growth of *A. alternata* on plates with zirconia and mixed oxides additives at a concentration of 0.001 wt%. Finally, Fig. 7 shows the % Inhibition of both fungi with all the additives synthesized.

As is shown in Fig. 7, in general, *C. globosum* strain evidenced to be more resistant than *A. alternata* for low concentrations, all samples in contact with the first one showed no inhibition at the lowest concentration. On the other hand, most samples showed a 100% of Inhibition when the concentration was of 0.05% w/v, that indicates that not only the Ag-additives presented antifungal activity but also additives without Ag in their composition inhibited the fungal growth. Only zirconia additives and the mixed oxide synthesized with PMA as catalyst (Figs. 6c and g) did not show that effect, probably due to the destruction of the PMA structure that enhance the fungal growth. The siliceous additives with acetic acid (SA and SA-Ag) and PMA as catalyst (SH and SH-Ag) showed a similar behavior against both fungi, showing an increase in % Inhibition values with Ag-additives. Finally, against *A. alternata*, when silver was absent in silica samples (SA and SH), the most acidic sample with the higher % inhibition at a concentration of 0.01% w/v was obtained.

The Ag-siliceous materials improve their antifungal activity when the Zr was introduced showing a higher antifungal activity at lower concentration. This can be seen in Fig. 7 comparing the % inhibition of SA-Ag and SH-Ag with SZA-Ag and SZH-Ag at the concentrations of 0.001% and 0.01% against both fungi *A. alternata* and *C. globosum*, respectively.

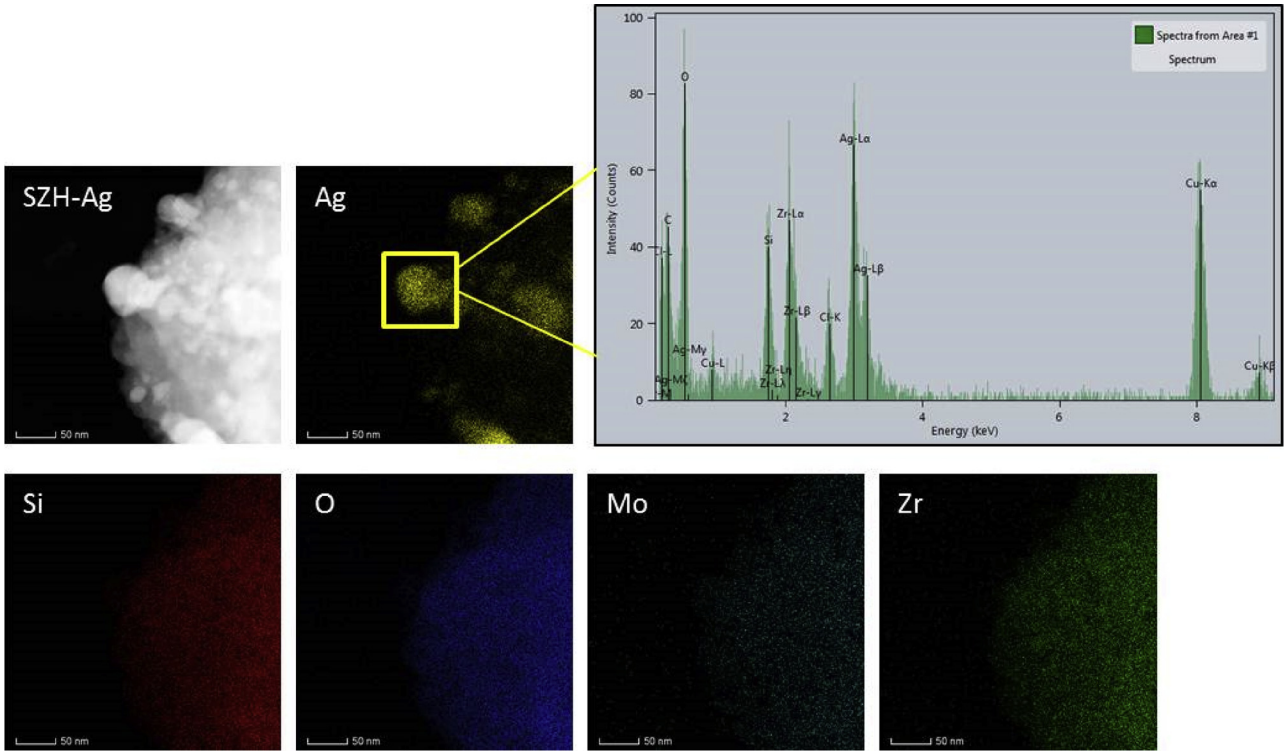

Fig. 5. Elemental mapping by scanning transmission electron microscopy of SZH-Ag sample, showing: silver, silicon, oxygen and zirconium.

3.3. Coatings bio-resistance assay

After the evaluation of the solids, and in accordance with the previous results, we selected 6 samples (SA, SH-Ag, ZA, ZH-Ag, SZA and SZH-Ag) to be incorporated as additives in water-borne paints due to their higher antifungal activity. After the selection, the bio-resistance of the paints was evaluated employing the standard method ASTM D5590. The results of this assay are shown in Fig. 8. The control paint (P control) and the others containing the additives without Ag (P SA, P ZA and P SZA) showed significant differences compared with the paints containing Ag, showing a mycelium development covering more than 60% of the exposed surfaces and evidencing no major inhibition against both fungal strains. Paints with SH-Ag, ZH-Ag and SZH-Ag additives (P SH-Ag, P ZH-Ag and P SZH-Ag, respectively), were highlighted showing a fungal growth degree less than those without Ag with a higher inhibition effect.

SEM micrographs, which are attached as Supporting Information (Figs. S3 and S4), showed in detail the paint film inoculated with *C. globosum* and *A. alternata*, respectively, after 4 weeks of incubation. The fungal development on paints P SA, P ZA and P SZA was higher with both strains and showed a high degree of sporulation. Furthermore, in P ZA and P SZA paints against *A. alternata* was particularly evident the active fungal growth with an important hyphae network. On the other hand, the micrographs of P SH-Ag, P ZH-Ag and P SZH-Ag paints only presented spores from inoculation without germination.

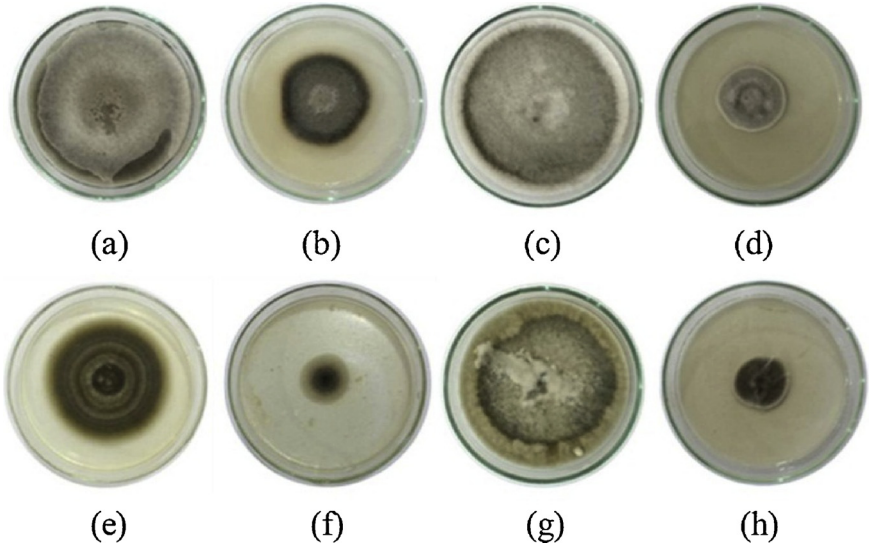

Fig. 6. Effect of the zirconia and mixed oxides additives at a concentration of 0.001 wt% on the fungal growth of *A. alternata* after 10 days at 26 °C, (a) ZA, (b) ZA-Ag, (c) ZH, (d) ZH-Ag, (e) SZA, (f) SZA-Ag, (g) SZH and (h) SZH-Ag.

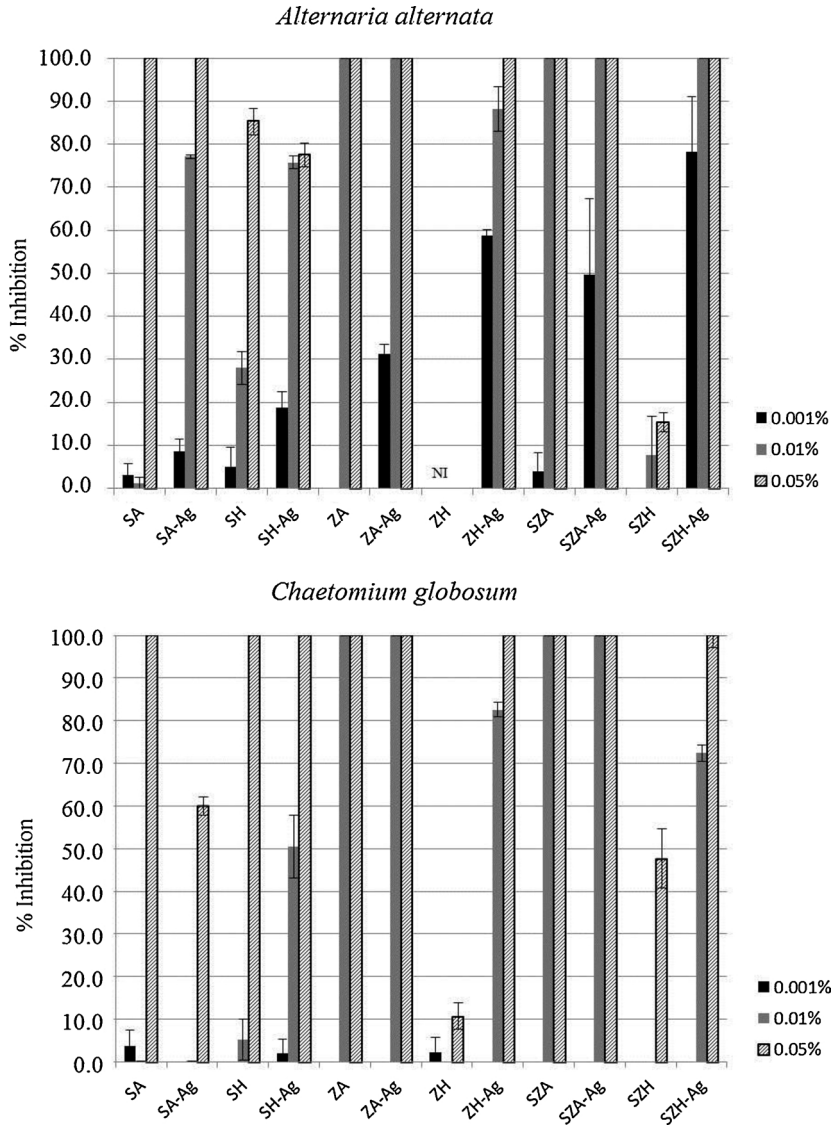

Fig. 7. Inhibition (%) of additives, against *A. alternata* and *C. globosum.* NI = No inhibition.

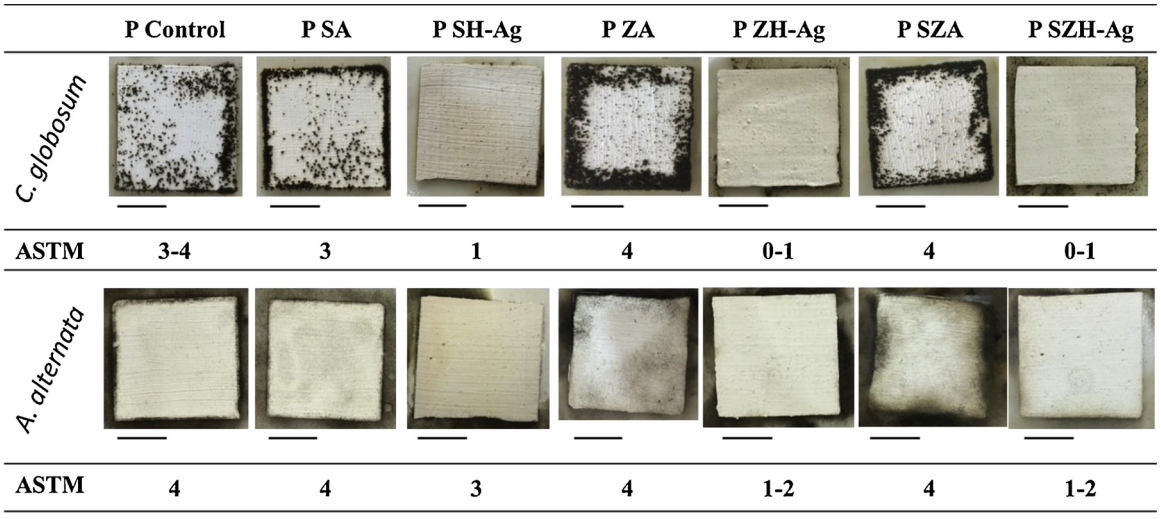

Fig. 8. Coating bio-resistance assay against *C. globosum* and *A. alternata.* Bar: 1 cm.

3.4. Color parameters and gloss determinations

The measurement of the color parameters shows that there are differences from the begging of the exposure assay among the paints and with the control. The main differences were seen in paint P SH-Ag, as L*, a* and b* values were 86.7, 4.74 and 10.1, respectively, giving the paint a reddish color. The other paints have values of L*, a* and b* around 95, 0 and 2, respectively (Supplementary Information S5).

During the exposure of the films for 100 days to sunlight behind a window the color changes in an important way in the cases of the paint containing silver, mainly in P SH-Ag and P SZH-Ag. When the panels were exposed to the darkness, only P SH-Ag changes its color with a ΔE rated as very evident (Supplementary Information S6). P SH-Ag changes mostly L* when it is exposed to the sunlight throw a window glass but in the darkness, the changes in color was mainly due to changes in a* and b*. The same happened with P SZH-Ag, L* changed in an important way when exposed behind the window but a* and b* changed in the darkness. This behavior indicates the different activity of silver depending on the exposure conditions and that not only it is affect by sunlight. The variations of L* (L* = 0 means lack of lightness) may indicate the formation and decomposition of black compounds as those formed when silver reacts with sulfur compounds, present in the environment [54]. The increased of L* may be due to the degradation of these compounds by light or O_3 [55]. The gloss of the paints was almost constant, around 2, value common for ceiling paints (IRAM 1109).

4. Conclusions

In the present work we try to develop new functionalized materials based on silicon dioxide (silica), zirconium oxide (zirconia), and mixed oxides (silica and zirconia) using different precursors and catalysts in the sol-gel synthesis. In order to impart antifungal activity, Ag particles were incorporated as part of functionalized process.

According to the antifungal evaluation of the additives, by agar plate inhibition test, it was observed that in order to the amount of solid added in the culture medium was increased, the percentage of inhibition was higher, whether was silver present or not in the solids, and producing in most samples a total inhibition of growth when the concentration was the maximum incorporated. The presence of Ag increased the percentage of inhibition in most of the samples, compared with the non-silver equivalents. Also, the more acidic samples gave the best results of inhibition, not being a direct dependence with the surface area values.

Against *C. globosum*, the samples showed the same behavior at the concentrations evaluated, and this fungus proved to be more resistant than *A. alternata* at low concentrations. Zirconia and mixed oxides synthesized with acetic acid and without Ag, showed inhibitory effects, but the incorporation of Ag in their composition exhibited better inhibition results against both fungal strains, notably inhibiting at the lowest concentration tested. The sample of mixed oxide synthesized with PMA led to not so good results against *C. globosum*, but the addition of Ag improved its inhibitory activity.

The inhibitory effect of the samples would be related first, to the presence of Ag and to their availability to interact with the microorganisms and second, to the acidity of the synthesized additives.

The synthesis of the mixed oxides (silica-zirconia) additives with the inclusion of Ag improved the antifungal activity performance, in comparison with the pure oxides (silica or zirconia), and a higher inhibition effect was registered against strains, *A. alternata* and *C. globosum*. In this sense, a synergic effect between zirconia/silica and silver would be a promising result that would allow reducing the amount of silver in these bioactive materials.

Acknowledgments

The authors wish to thank Mariela Theiller for providing the scanning electron microscopy images, Graciela Valle for FT-IR spectra, Pablo Fetsis for textural properties measures and Dr. Alberto Caneiro from Y-TEC (YPF Tecnología, Argentina) for his contribution to the HRTEM characterizations. This work was supported by National Scientific and Technical Research Council (CONICET), Comisión de Investigaciones Científicas de la Provincia de Buenos Aires (CICPBA) and National University of La Plata (UNLP).

Appendix A. Supplementary data

Supplementary material related to this article can be found, in the online version, at doi:https://doi.org/10.1016/j.porgcoat.2018.12.004.

References

[1] J.C.A. Janssens, H. Steenackers, S. Robijns, E. Gellens, J. Levin, H. Zhao, K. Hermans, D. De Coster, et al., Brominated furanones inhibit biofilm formation by *Salmonella enterica* serovar typhimurium, Appl. Environ. Microbiol. 74 (2008) 6639–6648, https://doi.org/10.1128/AEM.01262-08.

[2] A. Kramer, I. Schwebke, G. Kampf, How long do nosocomial pathogens persist on inanimate surfaces? A systematic review, BMC Infect. Dis. 6 (2006) 130–138, https://doi.org/10.1186/1471-2334-6-130.

[3] B. Little, R. Staehle, R. Davis, Fungal influenced corrosion of post-tensioned cables, Int. Biodeterior. Biodegrad. 47 (2001) 71–77, https://doi.org/10.1016/S0964-8305(01)00039-7.

[4] K.M. Usher, A.H. Kaksonen, I. Cole, D. Marney, Review Critical review: microbially influenced corrosion of buried carbon steel pipes, Int. Biodeterior. Biodegrad. 93 (2014) 84–106, https://doi.org/10.1016/j.ibiod.2014.05.007.

[5] K. Winkowski, Biocides for the coatings industry, in: A.A. Tracton (Ed.), Coatings Technology Handbook, CRC press Taylor & Francis group, Boca Raton FL, 2006pp 81-1/81-3.

[6] F. Siedenbiedel, J.C. Tiller, Review antimicrobial polymers in solution and on surfaces: overview and functional principles, Polymer 4 (2012) 46–71, https://doi.org/10.3390/polym4010046.

[7] M. Gouda, Nano-zirconium oxide and nano-silver oxide/ cotton gauze fabrics for antimicrobial and wound healing acceleration, J. Ind. Text 41 (2011) 222–240, https://doi.org/10.1177/1528083711414960.

[8] S. Gowri, R. Rajiv Gandhi, M. Sundrarajan, Structural, optical, antibacterial and antifungal properties of zirconia nanoparticles by biobased protocol, J. Mater. Sci. Technol. 30 (2014) 782–790, https://doi.org/10.1016/j.jmst.2014.03.002.

[9] S. Jaiswal, K. Bhattacharya, M. Sullivan, M. Walsh, B.S. Creaven, F. Laffir, B. Duffy, P. McHale, Non-cytotoxic antibacterial silver–coumarin complex doped sol–gel coatings, Colloids Surf. B Biointerfaces 102 (2013) 412–419, https://doi.org/10.1016/j.colsurfb.2012.07.047.

[10] H. Palza, B. Escobar, J. Bejarano, D. Bravo, M. Diaz-Dozque, J. Perez, Designing antimicrobial bioactive glass materials with embedded metal ions synthesized by the sol–gel method, Mater Sci. Eng. 33 (2013) 3795–3801, https://doi.org/10.1016/j.msec.2013.05.012.

[11] R. Arreche, K. Igal, N. Bellotti, P. Vázquez, Síntesis verde y caracterización de sólidos de matriz silícea con cobre y plata obtenidos a partir de dos precursores para su aplicación como aditivos antifúngicos, Revista Matéria 20 (2015) 612–620, https://doi.org/10.1590/S1517-707620150003.0062.

[12] L. Pinho, M. Rojas, M.J. Mosquera, Ag–SiO_2–TiO_2 nanocomposite coatings with enhanced photoactivity for self-cleaning application on building materials, Appl. Catal. B: Environ. 178 (2015) 144–154, https://doi.org/10.1016/j.apcatb.2014.10.002.

[13] C. Marambio-Jones, E.M.V. Hoek, A review of the antibacterial effects of silver nanomaterials and potential implications for human health and the environment, J. Nanopart. Res. 12 (2010) 1531–1551, https://doi.org/10.1007/s11051-010-9900-y.

[14] P. Singh, Y.J. Kim, C. Wang, R. Mathiyalagan, M. El-Agamy Farh, D.C. Yang, Biogenic silver and gold nanoparticles synthesized using red ginseng root extract, and their applications, Artif. Cells Nanomed. Biotechnol. 44 (2016) 811–816, https://doi.org/10.3109/21691401.2015.1008514.

[15] WHO, Silver in Drinking-water, Guidel. Drink. Qual. 2 (1996) 1-9. doi: WHO/SDE/WSH/03.04/96.

[16] P. Singh, Y.J. Kim, C. Wang, R. Mathiyalagan, D.C. Yang, The development of a green approach for the biosynthesis of silver and gold nanoparticles by using Panax ginseng root extract, and their biological applications, Artif. Cells Nanomed. Biotechnol. 44 (2016) 1150–1157, https://doi.org/10.3109/21691401.2015.1011809.

[17] J.R. Morones, J.L. Elechiguerra, A. Camacho, K. Holt, J.B. Kouri, J.T. Ramírez, M.J. Yacaman, The bactericidal effect of silver nanoparticles, Nanotechnology 16 (2005) 2346–2353, https://doi.org/10.1088/0957-4484/16/10/059.

[18] C. Lok, C. Ho, R. Chen, Q. He, Proteomic analysis of the mode of antibacterial action of silver nanoparticles, Proteome Res. 5 (2006) 916–924, https://doi.org/10.1021/pr0504079.

[19] P.Y. Chung, Y.S. Toh, Anti-biofilm agents: recent breakthrough against multi-drug resistant *Staphylococcus aureus*, Pathog. Dis. 70 (2014) 231–239, https://doi.org/10.1111/2049-632X.12141.

[20] M.J. Kasprowicz, M. Kozioł, A. Gorczyca, The effect of silver nanoparticles on

phytopathogenic spores of *Fusarium culmorum*, Can. J. Microbiol. 56 (2010) 247–253, https://doi.org/10.1139/W10-012.
[21] K.J. Kim, W.S. Sung, B.K. Suh, S.K. Moon, J.S. Choi, J.G. Kim, D.G. Lee, Antifungal activity and mode of action of silver nano-particles on Candida albicans, BioMetals. 22 (2009) 235–242, https://doi.org/10.1007/s10534-008-9159-2.
[22] C. Mitra, P.M. Gummadidala, K. Afshinnia, R.C. Merrifield, M. Baalousha, J.R. Lead, A. Chanda, Citrate-coated silver nanoparticles growth-independently inhibit aflatoxin synthesis in Aspergillus parasiticus, Environ. Sci. Technol. 51 (2017) 8085–8093, https://doi.org/10.1021/acs.est.7b01230.
[23] G. Sørensen, A.L. Nielsen, M.M. Pedersen, S.D. Nygaard, Controlled release of biocide from silica microparticles in wood paint, Prog. Org. Coat 68 (2010) 299–306, https://doi.org/10.1016/j.porgcoat.2010.03.009.
[24] N. Bellotti, R. Romagnoli, C. Quintero, C. Domínguez-Wong, F. Ruiz, C. Deyá, Nanoparticles as antifungal additives for indoor water borne paints, Prog. Org. Coat 86 (2015) 33–40, https://doi.org/10.1016/j.porgcoat.2015.03.006.
[25] R.A. Samson, E.S. Hoekstra, J.C. Frisvad, Introduction to Food and Airborne Fungi, 7th edn., (2004) CBS, Netherlands.
[26] C. Yang, D. Li, C. Yang, P.A. Heinsohn, Sampling and Analysis of Indoor Microorganisms, John Wiley & Sons, New Jersey, 2007.
[27] C.G.A. Olaf, R.A. Samson, Fundamentals of Mold Growth in Indoor Environments and Strategies for Healthy Living, Wageningen Academic Publishers, Netherlands, 2011.
[28] ASTM D5590-00, Standard Test Method for Determining the Resistance of Paint films and Related Coatings to Fungal Defacement by Accelerated Four-Week Agar Plate Assay.
[29] A. Popa, V. Sasca, E.E. Kiss, R. Marinkovic-Neducin, M.T. Bokorov, I. Holclajtner-Antunovic, Studies in structural characterization of silica–heteropolyacids composites prepared by sol–gel method, Mater. Chem. Phys. 119 (2010) 465–470, https://doi.org/10.1016/j.matchemphys.2009.09.026.
[30] R. Arreche, N. Bellotti, M. Blanco, P. Vázquez, Improved antimicrobial activity of silica–Cu using a heteropolyacid and different precursors by sol–gel: synthesis and characterization, J. Solgel Sci. Technol. 75 (2015) 374–382, https://doi.org/10.1007/s10971-015-3710-8.
[31] N. Bellotti, L. Salvatore, C. Deyá, M.T. Del Panno, B. del Amo, R. Romagnoli, The application of bioactive compounds from the food industry to control mold growth in indoor waterborne coatings, Colloids Surf. B Biointerfaces 104 (2013) 140–144, https://doi.org/10.1016/j.colsurfb.2012.11.037.
[32] J.H.C. Woudenberg, N.A. van der Merwe, Z. Jurjevic´, J.Z. Groenewald, P.W. Crous, Diversity and movement of indoor Alternaria alternata across the mainland USA, Fungal Genet. Biol. 81 (2015) 62–72, https://doi.org/10.1016/j.fgb.2015.05.003.
[33] C. Neukirch, C. Henry, B. Leynaert, R. Liard, J. Bousquet, F. Neukirch, Is sensitization to *Alternaria alternata* a risk factor for severe asthma? A population-based study, J. Allergy Clin. Immunol. 103 (1999) 709–711, https://doi.org/10.1016/S0091-6749(99)70247-2.
[34] C.J. Alexopoulos, C.W. Mims, Introducción a La Micología, Ed. Omega, 1. Ed, Barcelona (1985).
[35] I. Dosen, K.F. Nielsen, G. Clausen, B. Andersen, Potentially harmful secondary metabolites produced by indoor *Chaetomium* species on artificially and naturally contaminated building materials, Indoor Air 27 (2017) 34–46, https://doi.org/10.1111/ina.12290.
[36] E. Vági, B. Simándi, Á Suhajda, É Héthelyi, Essential oil composition and antimicrobial activity of Origanum majorana L. Extracts obtained with ethyl alcohol and supercritical carbon dioxide, Food Res. Int. 38 (2005) 51–57, https://doi.org/10.1016/j.foodres.2004.07.006.
[37] M. Özcan, N. Boyraz, Antifungal properties of some herb decoctions, Eur. Food Res. Technol. 212 (2000) 86–88, https://doi.org/10.1007/s002170000249.
[38] K.I. Suhr, P.V. Nielsen, Antifungal activity of essential oils evaluated by two different application techniques against rye bread spoilage fungi, J. Appl. Microbiol. 94 (2003) 665–674, https://doi.org/10.1046/j.1365-2672.2003.01896.x.
[39] G. Teichmann, The use of colorimetric methods in the concrete industry, Concrete Precasting Plant Technol. 11 (1990) 58–73.
[40] B. Ritzer, M.A. Villegas, J.M. Fernández Navarro, Influence of temperature and time on the stability of silver in silica sol-gel glasses, J. Solgel Sci. Technol. 8 (1997) 917–921, https://doi.org/10.1023/A:1018332929290.
[41] P. Villabrille, G. Romanelli, N. Quaranta, P. Vázquez, An efficient catalytic route for the preparation of silyl ethers using alumina-supported heteropolyoxometalates, Appl. Catal. B 96 (2010) 379–386, https://doi.org/10.1016/j.apcatb.2010.02.035.
[42] A. Popa, V. Sasca, M. Stefanescu, E.E. Kiss, R. Marinkovic-Neducin, The influence of the nature and textural properties of different supports on the thermal behavior of Keggin type heteropolyacids, J. Serb Chem. Soc. 71 (2006) 235–249, https://doi.org/10.2298/JSC0603235P.
[43] S.J. Gregg, K.S.W. Sing, Adsorption, Surface Area and Porosity, 2nd edn., Academic Press, London, 1982.
[44] S. Duhan, N. Kishore, P. Aghamkar, S. Devi, Preparation and characterization of sol-gel derived silver-silica nanocomposite, J. Alloys. Compd. 507 (2010) 101–104, https://doi.org/10.1016/j.jallcom.2010.07.107.
[45] M. Pakizeh, M.R. Omidkhah, A. Zarringhalam, Synthesis and characterization of new silica membranes using template sol-gel technology, Int. J. Hydrogen Energy 32 (2007) 1825–1836, https://doi.org/10.1016/j.ijhydene.2006.07.025.
[46] A. Durán, C. Serna, V. Fornes, J.M. Fernandez-Navarro, Structural considerations about SiO_2 glasses prepared by sol-gel, J. Non-Cryst. Solids 82 (1986) 69–77, https://doi.org/10.1016/0022-3093(86)90112-2.
[47] G. Orcel, J. Phalippou, L.L. Hench, Structural changes of silica xerogels during low temperature dehydration, J. Non-Cryst. Solids 88 (1986) 114–130, https://doi.org/10.1016/S0022-3093(86)80092-8.
[48] N. Agoudjil, S. Kermadi, A. Larbot, Synthesis of inorganic membrane by sol–gel process, Desalination 223 (2008) 417–424, https://doi.org/10.1016/j.desal.2007.01.187.
[49] Y. Sorek, M. Zevin, R. Reisfeld, Zirconia and zirconia-ORMOSIL planar waveguides prepared at room temperature, Chem. Mater. 9 (1997) 670–676, https://doi.org/10.1021/cm960135x.
[50] J.M. Hernández Enríquez, L.A. Cortez Lajas, R. García Alamilla, A. Castillo Mares, G. Sandoval Robles, L.A. García Serrano, Synthesis and characterization of mesoporous and nano-crystalline phosphate zirconium oxides, J. Alloys. Compd. 483 (2009) 425–428, https://doi.org/10.1016/j.jallcom.2008.08.094.
[51] P. Vázquez, M. Blanco, C. Cáceres, Catalysts based on supported 12-molybdophosphoric acid, Catal. Lett. 60 (1999) 205–215, https://doi.org/10.1023/A:1019071410838.
[52] N.F. Adegboyega, V.K. Sharma, K. Siskova, R. Zboril, M. Sohn, B.J. Schultz, S. Banerjeet, Interactions of aqueous Ag^+ with fulvic acids: mechanisms of silver nanoparticle formation and investigation of stability, Environ. Sci. Technol. 47 (2013) 757–764, https://doi.org/10.1021/es302305f.
[53] A. Babapour, O. Akhavan, R. Azimirad, A.Z. Moshfegh, Physical characteristics of heat-treated nano-silvers dispersed in sol–gel silica matrix, Nanotechnology 17 (2006) 763–771, https://doi.org/10.1088/0957-4484/17/3/025.
[54] F.A. Cotton, G. Wilkinson, Química Inorgánica Avanzada, 4th Edition, Limusa Noriega publisher, 1980 p1165.
[55] Sidgwick NV, Los elementos químicos y sus compuestos, Aguilar publisher, p123-135.